약학석사학위논문

Biocompatible graphene nanosheets tethered with poly-gamma glutamic acid for anticancer therapy

Poly-gamma glutamic acid 가 코팅된 생체적합 그래핀 나노시트를 이용한 항암치료

2016 년 8 월

서울대학교 대학원

분자의학 및 바이오제약학과

문 희 원

Abstract

Here, I report that poly gamma glutamic acid (γ-PGA)-modified graphene could improve hemocompatibility and biocompatibility for enhanced in vivo safety and therapeutic index of graphene-based nanomedicine. Phenylalanine-grafted γ-PGA (amphiphilic γ-PGA , APGA) was synthesized and coated on reduced graphene oxide (rGO) via non-covalent interaction resulting APGA-coated rGO (ArGO). Modification of APGA on rGO did not interrupt photothermal activity of rGO, showing similar increase of temperature upon near-infrared (NIR) laser irradiation. ArGO revealed prolonged dispersion stability under physiological fluids over 4weeks whereas rGO in a plain form or physical mixture with γ-PGA was immediately deposited under same conditions. Although rGO in a plain form or physical mixture with γ-PGA form aggregation with red blood cells from at a rGO dose of 31mg/l ArGO showed much higher hemocompatibility upto rGO dose of 250 mg/l. Adding of γ-PGA did not decrease acute lethal rate of rGO, resulting 0 % survival rate at a rGO dose of 50 mg/kg, however, ArGO showed 100% survival rate of animals after intravenous injection at a same dose. Systemic administration of ArGO facilitated prolonged blood retention of

rGO over 8 h post-dosing and significantly enhanced tumor accumulation in SCC7 tumor-bearing mice at 24 h post-dosing as compared with rGO-treated mice which resulting temperature increase to 50.2 ± 0.7^{o}C at tumor sites upon NIR laser irradiation. Single irradiation of ArGO-treated mice revealed tumor ablation effect whereas tumor volumes of untreated and rGO-treated mice rapidly grew. Our results provides an evidence that biocompatible graphene via non-covalent modification of APGA would potentiate clinical applications of graphene-based nanomedicine.

Keywords: Poly gamma glutamic acid derivative, Graphene nanosheets, Reduced graphene oxide, Surface functionalization, In vivo safety, Photothermal therapy, Anticancer therapy

Student number : 2014-24865

Contents

V. Conclusion

VI. Reference

List of Figures

1. Introduction

Graphene nanosheets have been regarded as an emerging nanocarrier modality for anticancer therapy due to its distinctive characteristics [Orecchioni et al., 2015]. Although structural properties of graphene offer diverse virtues such as high loading capacity for cargo drugs [Shen et al., 2012], photothermal activity [Miao et al., 2014], and multi-modification capability [Wang et al., 2013], graphene nanosheets suffer from low hemocompatibility [Sasidharan et al., 2012], and biocompatibility [Duch et al., 2011; Xu et al., 2015; Jachak et al., 2012] after in vivo administration.

Thus, extensive stabilizing agents have been studied to improve stability of graphene under physiological conditions via covalent or non-covalent modification of graphene surfaces including polysaccharides [Shim et al., 2014], polymers [Miao et al., 2013a; Li et al., 2014], and proteins [Sheng et al., 2013]. It would be preferable for stabilization of graphene to consider whether stabilizing biomolecules did not disrupt innate characteristics of graphene. Theoretical installation of tethering moiety for graphene is also required for rational design of biocompatible graphene since rapid dissociation of biomolecules from graphene can

occur according to nonspecific weak adsorption [Rajesh et al., 2009; Kim et al., 2011].

Poly gamma glutamic acid (γPGA) is an anionic and water-soluble biopolymer with unique peptide bonds between α-amino group and the γ-carboxyl group [Ogunleye et al., 2015]. Due to its biodegradable, and non-immunogenic characteristics, γPGA has been extensively exploited for food, cosmetic, healthcare, and medical applications [Bajaj and Singhal, 2011]. Interestingly, various bacterial strains spontaneously produce these poly amino acids on their surfaces to protect themselves from host defense such as antimicrobial peptides and neutrophil phagocytosis [Kocianova 2005; Foster et al., 2005; Scorpio 2007; Jang et al., 2011]. Therefore, modification of γPGA on graphene surfaces deserves consideration due to its physicochemical properties and innate functionality as a biocapsule.

Here, I formulated biocompatible graphene for improved in vivo safety and therapeutic index of graphene-based nanocarriers. I demonstrated that non-covalent modification of γPGA on reduced graphene oxide (rGO) via phenylalanine anchoring moiety provides prolonged stability under physiological fluids, enhanced tumor

accumulation, and photothermal anticancer effect in SCC7 tumor-bearing animal model.

2. Materials and methods

2.1 Synthesis of amphiphilic γ-PGA derivative

Amphiphilic derivative of γ-PGA (50 kDa) was synthesized by conjugating amino group of phenylalanine ethyl ester with the carboxyl groups of γ-PGA. γ-PGA (297 mg, 5.94 μmol, Bioleaders Corp., Daejeon, Republic of Korea) was dissolved in 30 ml of 0.3 M aqueous sodium bicarbonate (Sigma Aldrich, St. Louis, MO, USA), and added dropwise with N-(3-dimethylaminopropyl)-N′-ethylcarbodiimide hydrochloride (441 mg, 2.3 mmol, Sigma Aldrich) in 10 ml of 0.3 M aqueous $NaHCO_3$. The solution was then stirred at 0^oC for 30 min and slowly added with powder of L-phenylalanine ethyl ester hydrochloride (528 mg, 2.3 mmol, Sigma Aldrich). After 12 h of stirring at room temperature, the reaction mixture was dialyzed against triple distilled water (TDW) for 48 h and methanol for 48 h. After removal of methanol by distillation under reduced pressure, the resulting amphiphilic L-phenylalanine ethyl ester-grafted-γ-PGA (PhePGA) products were dissolved in TDW, lyophilized, and characterized by ^1H NMR.

2.2 Preparation of rGO nanosheets

rGO nanosheets were prepared by reducing GO nanosheets. GO nanosheets were prepared from graphite using Hummer's method with slight modification (Miao et al., 2015). In brief, for synthesis of rGO nanosheets, 2.0 ml of GO nanosheets (5 mg/ml) in triple-distilled water (TDW) was added with 8.0 ml of TDW, 0.5 ml of ammonia solution (28 w/w% in water, Junsei Chemical, Tokyo, Japan), 5.0 μl of hydrazine monohydrate (64 w/w% in water, Sigma-Aldrich). The resultant mixture was stirred at 80^{o}C for 10 min. After cooling down to room temperature, the excess hydrazine and ammonia was removed by dialysis (MWCO 100K; Spectrum Laboratories, Inc., Rancho Dominguez, CA, USA) against TDW. The obtained rGO nanosheets were stored at 4 ^{o}C until use.

2.3 Preparation of PHEPGA coated rGO nanosheets

For surface coating with PHEPGA, rGO nanosheets in TDW (1 mg/ml) was mixed with the same volume of PHEPGA solution (2 mg/ml) by vigorous shaking for 2 min, and incubated at room temperature for 5

min. PHEPGA-coated rGO (ArGO) was identified by fourier transform infrared spectroscopy (FT-IR) analysis (FT/IR-4200, JASCO International Co., Ltd., Tokyo, Japan).

2.4 Size and zeta potential measurement

The morphology and lateral sizes of the generated nanosheets were measured using transmission electron microscopy and dynamic light scattering, respectively. The morphology of nanosheets was examined by a transmission electron microscope (JEM1010; JEOL Ltd, Tokyo, Japan). The rGO or ArGO nanosheets were diluted with TDW and placed in an ELS-Z (Photal, Osaka, Japan). The hydrodynamic diameters of the nanosheets were determined by He-Ne laser (10 mW) light scattering, and the zeta potential values of rGO and ArGO nanosheets were determined using an ELS-8000 instrument (Photal).

2.5 Stability in physiological conditions

The stability of rGO, ArGO, and mixture of γ-PGA and rGO nanosheets was tested in various environments. For mixture of γ-PGA and rGO nanosheets, rGO nanosheets in water (1 mg/ml) was mixed with the

same volume of γ-PGA solution (2 mg/ml). An aliquot (0.2 ml) of each group in TDW was added to 0.8 ml of phosphate buffered saline (PBS, 150 mM, pH 7.4), RPMI media or mouse serum, and the solutions were allowed to stand for 4 weeks. The stability of ArGO nanosheets was evaluated during this period by monitoring the appearance of precipitates using a digital camera (Canon PC1089, Canon Inc, Tokyo, Japan).

2.6 Animals

In vivo experiments were conducted using five week old female Balb/c or Balb/c athymic nude mice supplied by Orient Bio. Lab. Animal Inc. (Seungnam, Kyonggi-do, South Korea, Approved animal experimental protocol number: SNU-130129-3-4). Animals were raised under standard pathogen-free conditions at the Animal Center for Pharmaceutical Research in the Seoul National University. All animal experiments were conducted in accordance with the Guidelines for the Care and Use of Laboratory Animals of the Institute of Laboratory Animal Resources, Seoul National University.

2.7 Red blood cell aggregation assay

Red blood cell (RBC) aggregation assay was performed using a 5-week-old female Balb/c mice from Orient Bio, Inc. Animals were sacrificed using CO_2 and blood was extracted from heart. Blood (5 ml) was washed with 35 ml of fresh PBS for three times by centrifuging at 900 xg, 4°C for 10 min. RBC pellets were suspended in 175 μl of PBS, and added with 25 μl of rGO (1 mg/ml) in plain form, ArGO, or in mixture with γ-PGA (2 mg/ml). The maximum concentration of rGO was 125 μg/ml (PHEPGA 250 μg/ml) and the samples were serially diluted by half. The plate was observed at 37°C for 1 hour by monitoring the aggregation of RBC using a digital camera (Canon PC1089).

2.8 Acute toxicity tests of rGO and ArGO nanosheets

For acute toxicity test, 5-week-old female Balb/c mice were obtained from Orient Bio, Inc. Various amounts of rGO, γ-PGA+rGO or ArGO nanosheets were dispersed in 5% glucose solution and intravenously injected into the tail veins of mice. The survival of mice at 24 h post-injection was recorded for each group (n = 5).

2.9 Pharmacokinetic study

To determine the pharmacokinetic profiles of rGO and ArGO, mice were intravenously administered with 1,2-distearoyl-sn-glycero-3-phosphoethanolamine-N-[poly(ethyleneglycol)5000-Alexa680 (DSPE-PEG5000-Alexa680)-labeled rGO or ArGO at an rGO dose of 5 mg/kg. The rGO was labeled with DSPE-PEG5000-Alexa680, as described previously (Shim et al., 2014). The blood samples were collected at various time points after dosing. The fluorescence intensities of blood were measured using an eXplore Optix system (Advanced Research Technologies Inc., Montreal, Canada). The excitation and emission spots were raster-scanned in 1-mm steps over the region of interest to generate emission wavelength scans. A 670nm pulsed-laser diode was used to excite Alexa680 molecules. Long wavelength fluorescence emission (600–700 nm) was detected with a fast photomultiplier tube (Hamamatsu Photonics, Hamamatsu, Japan) and a time-correlated single photon counting system (Becker and Hickl GmbH, Berlin, Germany). Finally, the non-compartmental pharmacokinetic parameters were calculated with the software program WinNonlin^{TM} (Scientific Consulting Inc., Lexington, KY, USA). The mean residence time (MRT) was calculated by the non-compartmental method dividing

the area under the momentum curve (AUMC) with the area under the curve (AUC).

2.10 In vivo molecular imaging

Biodistribution of rGO or ArGO to tumor tissues was tested by molecular imaging. Mice were subcutaneously inoculated at right dorsal side with 3×10^6 SCC7 cells, and tumors were allowed to grow over time. DSPE-PEG5000-Alexa680-labeled rGO or ArGO was intravenously administered at an rGO dose of 5 mg/kg to SCC7-bearing mice. At 1 or 24 h post-dose, the tumor tissue distribution of fluorescent rGO or ArGO was assessed using an eXplore Optix system (Advanced Research Technologies Inc.) as described above.

2.11 In vivo photothermal tumor ablation study

The photothermal anticancer effects of rGO and ArGO were tested using SCC7 tumor-bearing nude mice. Five-week-old athymic nude mice (Orient Bio, Inc.) were subcutaneously injected at the dorsal right side with 3×10^6 SCC7 cells. On day 6, the mice were subjected to intravenous

administration of rGO or ArGO at an rGO dose of 5 mg/kg. One day post-administration, the mice were anesthetized and positioned in a mouse holder. The tumor sites were irradiated with an 808nm continuous-wave NIR laser at an output power of 1.5 W for 3 min. Light induced temperature change in tumor region was recorded using a real-time infrared thermal imaging system (FLIR T420, FLIR Systems Inc, Danderyd, Sweden). Tumor size were measured in two dimensions using a slide caliper, and the tumor volume as $a \times b^2 \times 0.5$, where a is the largest and b is the smallest diameters. In some experiments, tumor tissues were extracted on day 7 after the first inoculation of tumor cells, fixed in 10% neutral buffered formalin, and embedded in paraffin blocks for further histological evaluation. Tumor tissue sections (4 μm thick) were immunostained with an anti-proliferating cell nuclear antigen (PCNA) antibody (Thermo Fisher Scientific) to determine cell-proliferation status and assayed for apoptosis by terminal deoxynucleotidyl transferase dUTP nick-end labeling (TUNEL) (Millipore Corporation). The numbers of proliferating and apoptotic cells were counted using Image-Pro Plus Version 6.0 image analysis software (Media Cybernetics, Inc., Rockville,

MD, USA) after photographing five different fields at a magnification of 200x using an Eclipse TE2000-S microscope (Nikon, Tokyo, Japan).

2.12 Statistics

ANOVA was used for statistical evaluation of experimental data, using Student-Newman-Keuls test for a post-hoc test. All statistical analyses were done using the SigmaStat software (version 3.5, Systat Software, Richmond, CA, USA), and a p-value < 0.05 was considered significant.

III. Results

3.1 Synthesis and characterization of APGA

APGA was synthesized by the condensation of the amine group of phenylalanine ethyl ester and carboxyl group of γ-PGA (Suppl. Fig. 1A). As shown in Suppl. Fig. 1B, the peaks of chemical shift from 7.2 to 7.4 showed the presence of phenyl moiety in final APGA product. The peaks of chemical shift from 1.8 to 2.4 are attributed to the methylene of γ-PGA. The grafting ratio of phenylalanine ethyl ester was 25.89 ± 0.5 %.

Fig. 1. Synthesis scheme and characterization of APGA.

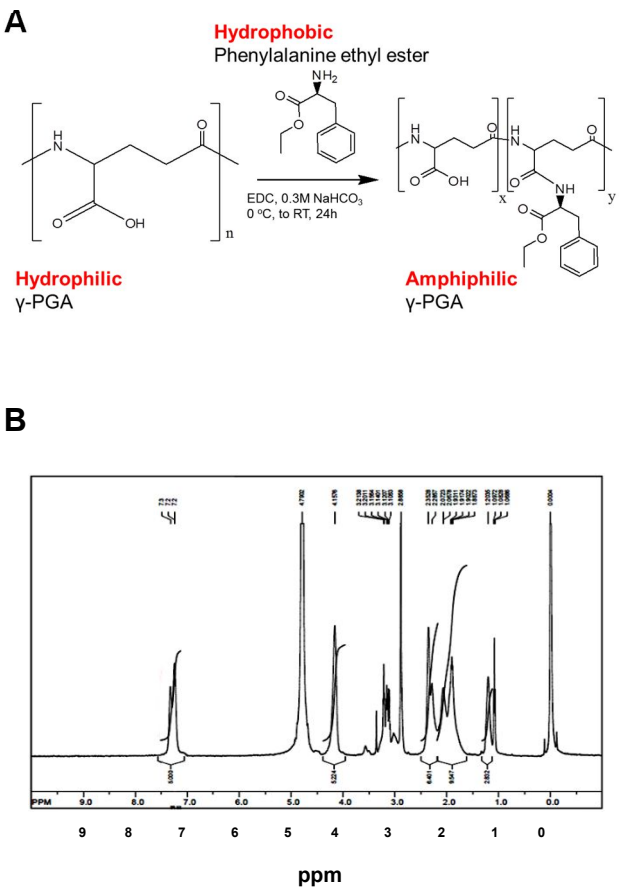

Fig. 1. Synthesis scheme and characterization of APGA.

(A) Synthesis scheme of APGA is described. (B) ^{1}H NMR data was obtained for APGA.

3.2 Characterization of ArGO nanosheets

APGA was coated onto the surface of rGO nanosheets by π-stacking interaction as illustrated in Fig. 1A. The rGO (Fig. 1B) and ArGO (Fig. 1C) nanosheets did not reveal particular differences in morphology. The FT-IR spectrum of rGO showed the two weak absorption bands at 1215 and 1573 cm^{-1} corresponding to C-C and C=C aromatic stretching vibrations (Fig. 1D) [Wang et al., 2013b]. In the spectrum of ArGO, several characteristic bands of APGA at 1205, 1387, 1550, 1642, and 1727 cm^{-1} which represent C-O in esters, N-H/C-N, COO-, C=O in amides and carboxylic acids [Yuan et al., 2014] indicated the presence of APGA in final product. The lateral size of ArGO nanosheets was also not differ from that of rGO nanosheets, showing 114.1 ± 4.1 and 106.1 ± 6.5 nm, respectively (Fig. 1E). The zeta potential values of nanosheets were decreased after loading of APGA onto rGO (Fig. 1F). Coating of APGA on rGO had no influence on photothermal activity of rGO, exhibiting the increase of temperature as 18.1 ± 0.5^{o}C (ArGO) and 16.8 ± 0.6 ^{o}C (rGO) with a rGO concentration of 20 μg/ml upon NIR laser irradiation (Fig. 2).

Fig. 2. Characterization of ArGO nanosheets.

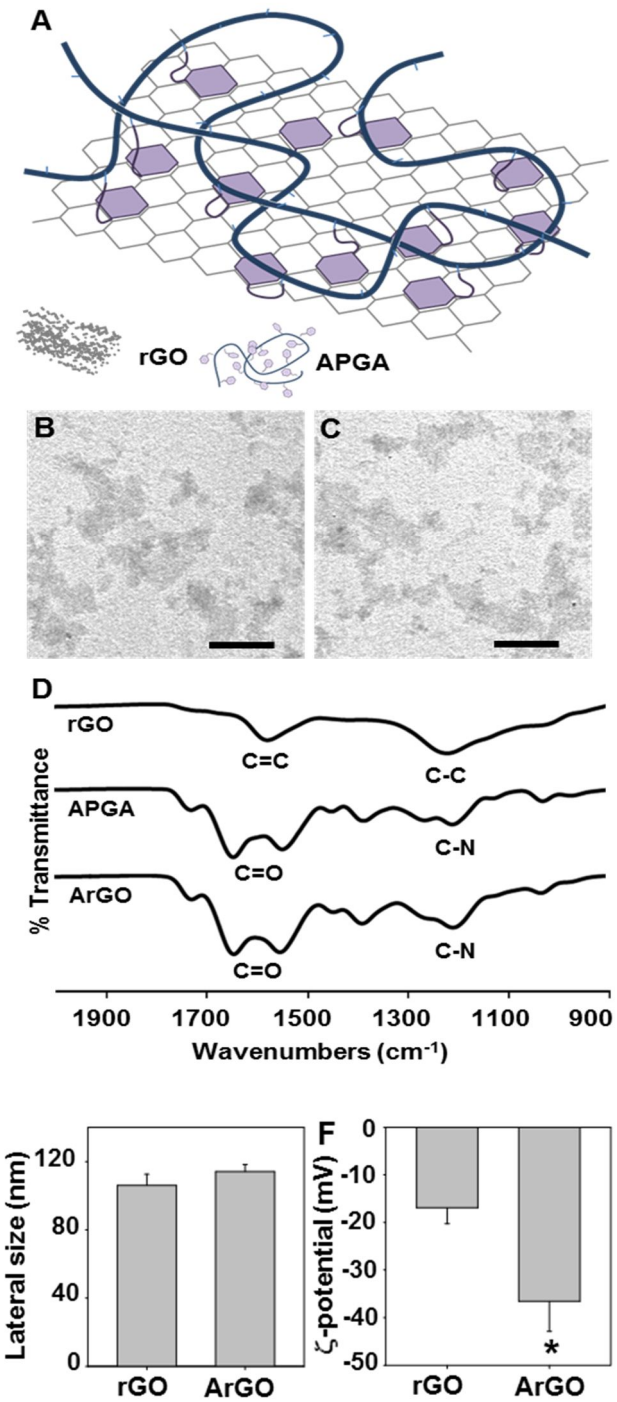

The schematic illustration of ArGO is shown in (A). TEM images of rGO (B) and ArGO (B) were obtained. (D) FT-IR spectra of rGO, APGA, and ArGO are presented.

(E) The lateral diameters of rGO and ArGO were measured by dynamic light scattering. (F) The zeta potentials were determined using an electro-Doppler method. Scale bar, 100 nm. *Significantly lower ($p < 0.05$) compared to the rGO-treated group (assessed by t-test).

3.3 Stability and safety of ArGO nanosheets

ArGO showed higher stability in various physiological conditions compared with rGO nanosheets (Fig. 3A). After dispersion in saline buffer, culture media, or mouse serum, the ArGO nanosheets with a weight ratio of 2:1 (APGA:rGO) did not form any precipitates and this appearance was maintained above 4 weeks whereas the rGO nanosheets in a plain form or physical mixture with γPGA (γPGA:rGO=2:1, w/w) immediately showed the aggregation. Fig. 3B shows the stability of rGO, γPGA+rGO, and ArGO in blood with different concentrations of rGO. As shown, the RBC aggregation in rGO and γPGA mixed rGO group were prominent enough to see within 1 hour. However, in ArGO group, the high hemoconpatibility was confirmed by showing no aggregation of RBC. Safety profile of ArGO was significantly different from that of rGO nanosheets in a plain form or physical mixture with γPGA (Fig. 3C). The survival rate was 40 % or 20 % when the mice were intravenously administered with rGO or γPGA mixed rGO nanosheets at a dose of 40 mg/kg, respectively, and decreased to 0 % at 40 mg/kg. Administration of ArGO nanosheets revealed the 100 % of survival rate up to rGO dose of 50 mg/kg (Fig. 3C).

Fig. 3. Biocompatible properties of ArGO nanosheets.

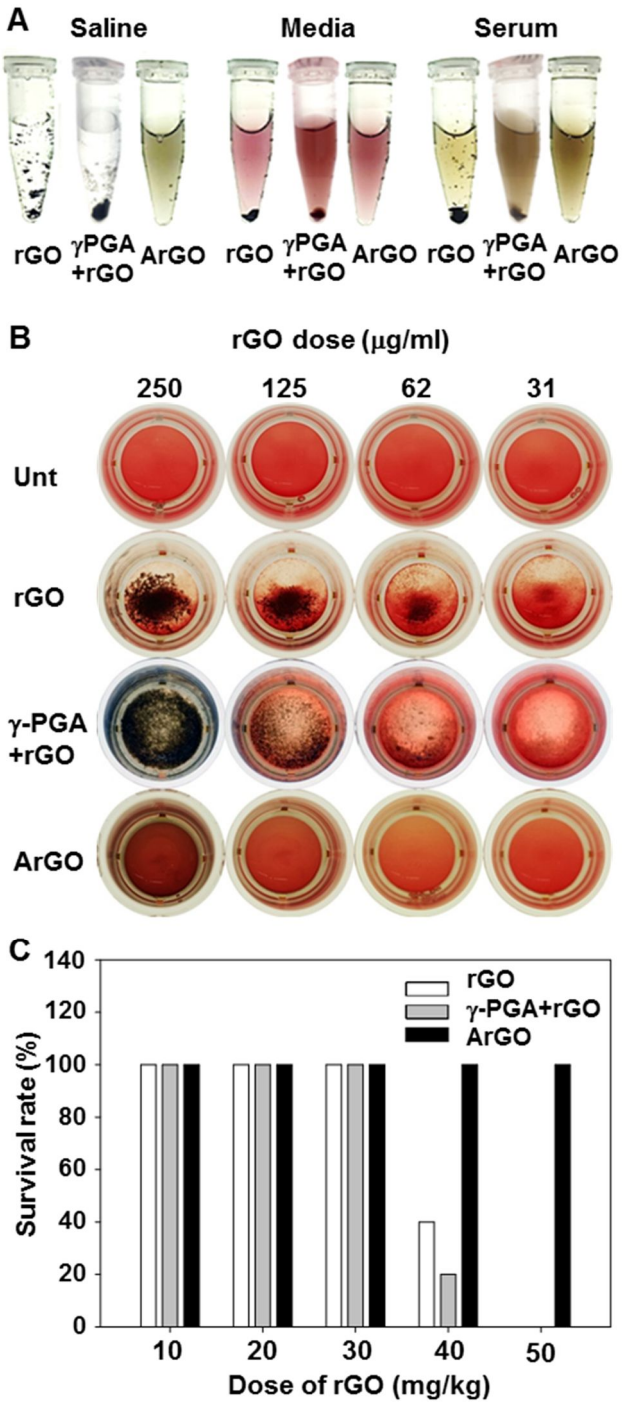

(A) The stability of rGO, γPGA+rGO, and ArGO nanosheet suspensions was observed after 4 weeks post-dispersion in PBS, media or serum. (B) Aggregation of RBCs was monitored at 1 h after (C) Balb/c mice were intravenously injected with various doses of rGO or ArGO nanosheets (n = 5), and survival was assessed 1 day later.

3.4 Pharmacokinetic profile

ArGO nanosheets differed from rGO nanosheets in pharmacokinetic profiles following intravenous administration to mice. When the mice were administered with rGO nanosheets at a dose of 5 mg/kg, detection level of rGO was rapidly decreased immediately after injection (Fig. 4). As compared to rGO, ArGO showed significantly higher retention in bloodstream over 8 h. The AUC value of ArGO was 37814.7 $\pm$ 3363.0 (photon counts h/ml), 2-fold higher than that of rGO nanosheets.

Fig. 4. In vivo biodistribution of ArGO nanosheets.

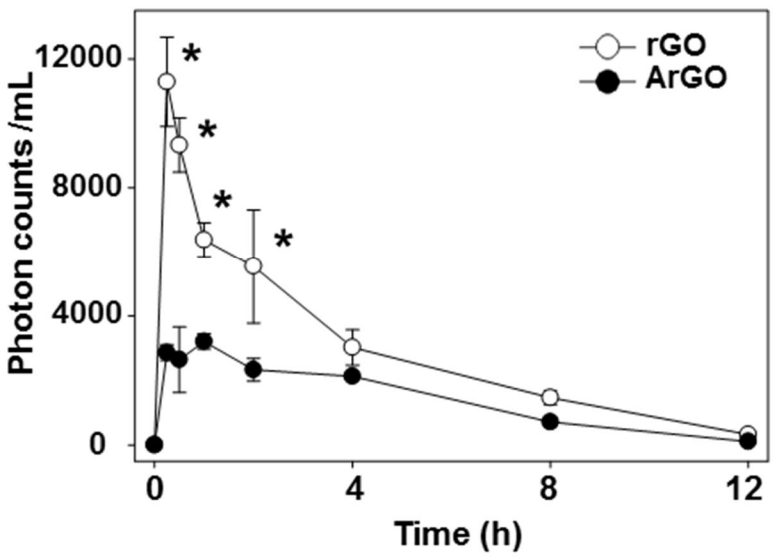

(A) SCC7-bearing mice were systemically treated with DSPE-PEG_{5000}-Alexa Fluor680 modified rGO or ArGO. After 24 h, the in vivo distributions of Alexa Fluor®680 fluorescence were visualized using a molecular imaging system. The tumor sites are indicated by the red dotted circles. (B) Average photon counts at tumor site were quantified by in vivo imaging system. The results are the mean ± SD of three independent experiments. *Significantly higher ($p < 0.05$) compared to the rGO/Dox group (assessed by ANOVA and the Student-Newman-Keuls test).

3.5. In vivo tumor tissue distribution of ArGO nanosheets

The tumor distribution of ArGO nanosheets was higher than that of rGO nanosheets after intravenous injection (Fig. 5). Although similar tumor accumulations were observed at 1 h post-administration of rGO or ArGO (Fig. 5A), the distribution at tumor sites was greater in the ArGO-treated mice than in the rGO-treated mice at 24 h after dosing (Fig. 5B). The ArGO-treated mice showed the increased fluorescence signal in tumor site after 24 h whereas rGO-treated mice remain the similar level of fluorescence in tumor sites with a time point of 1 h. The photon count measurements revealed that the tumor retention of ArGO nanosheets was 1.4-fold higher than that of rGO nanosheet at 24 h after dosing (Fig. 5C).

Fig. 5. Photothermal antitumor effect of the ArGO nanosheets.

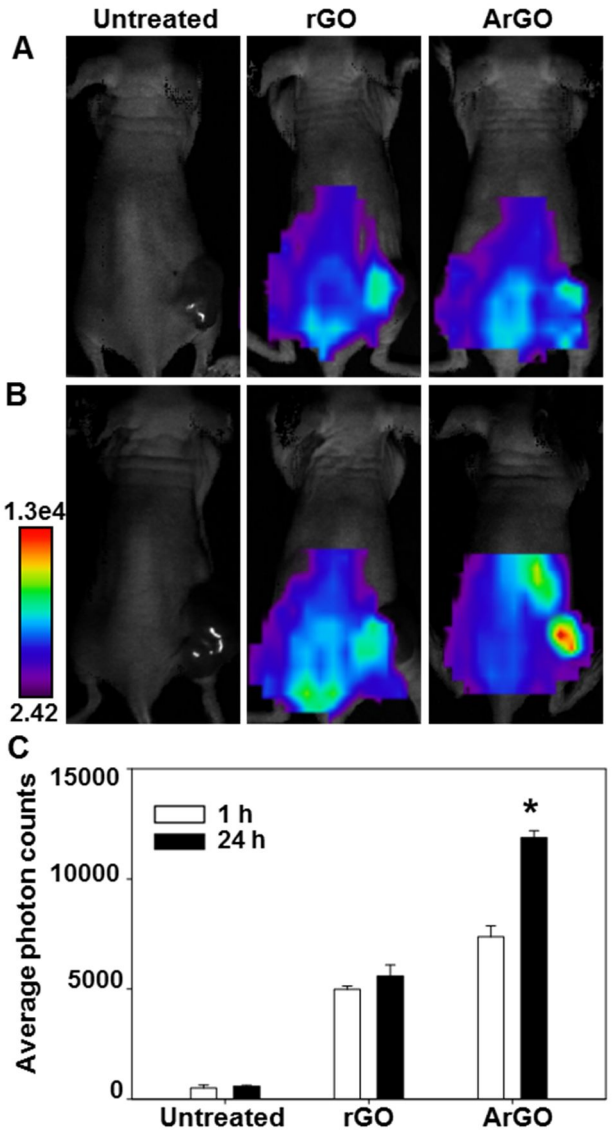

SCC7-bearing mice were intravenously treated with rGO or ArGO by administering a single injection on day 6. After 24 h, the tumor tissues

were irradiated with an 808 nm laser at a power density of 1.5 W/cm^2 for 3 min. (A) The real-time temperature changes at the tumor site were visualized by real-time infrared thermal imaging. (B) The average temperature of the tumor site was measured using the FLIR QuickReport 1.2 software. (C) On day 7, the appearances of the tumor sites of rGO or ArGO-treated mice were monitored. (D) The tumor volumes were periodically measured using calipers until day 19. *Significantly different ($p < 0.05$) from the other groups (assessed by the ANOVA and the Student–Newman–Keuls test).

3.6 In vivo photothermal antitumor effect of ArGO nanosheets

After systemic administration of ArGO to SCC7 tumor-bearing mice, the temperature increase of tumor sites was monitored by IR thermal imaging. One day post-treatment, the highest temperature was observed in the tumor tissues of ArGO-treated mice after 3 min of NIR laser irradiation (Fig. 6A). In this group, the temperature of tumor site was 50.2 ± 0.7^{o}C, which was 9.8^{o}C higher than rGO-treated group (Fig. 6B). One day after NIR irradiation, a black scab formed over the tumor site of ArGO-treated mice (Fig. 7B). After single irradiation on day 6, ArGO-treated mice revealed and maintained tumor ablation whereas rGO-treated group showed rapid growth with the tumor volumes similar to untreated group (Fig. 7C). Immunohistochemistry of tumor sections on day 7 demonstrated inhibition of tumor growth and apoptosis of tumor cells of ArGO-treated mice upon NIR irradiation (Fig. 8). The PCNA-positive cell population in tumor cells of ArGO-treated mice was 11.4- and 8.6-fold lower than untreated and rGO-treated mice, respectively (Fig. 8A, 8B). Oppositely, 6.0 or 2.9-fold higher apoptotic cell population was shown in tumor cells of ArGO-treated mice as compared than untreated or rGO-treated groups, respectively (Fig. 8A,

8C).

Fig. 6. Photothermal antitumor effect of the ArGO nanosheets.

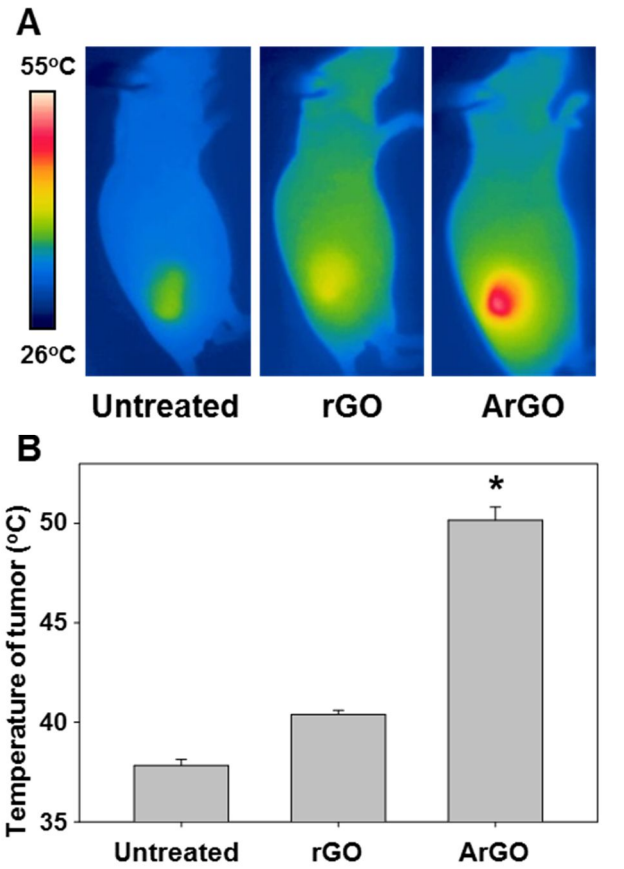

. SCC7-bearing mice were intravenously treated with rGO or ArGO by administering a single injection on day 6. After 24 h, the tumor tissues were irradiated with an 808 nm laser at a power density of 1.5 W/cm^2 for 3 min. (A) The real-time temperature changes at the tumor site were visualized by real-time infrared thermal imaging. (B) The average temperature of the tumor site was measured using the FLIR QuickReport

1.2 software. *Significantly different ($p < 0.05$) from the other groups (assessed by the ANOVA and the Student–Newman–Keuls test).

Fig. 7. Photothermal antitumor effect of the ArGO nanosheets

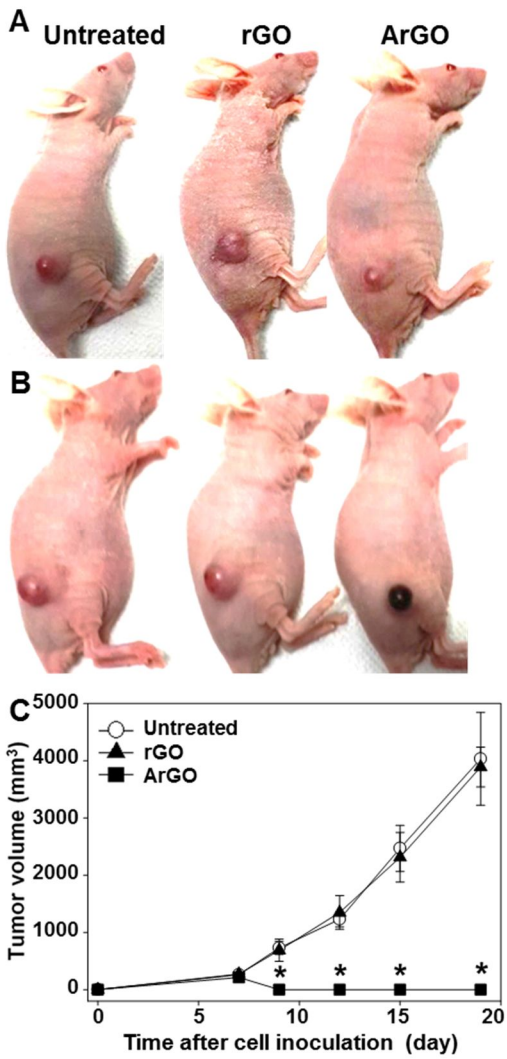

(A) SCC7-bearing mice were intravenously treated with rGO or ArGO by administering a single injection on day 6. After 24 h, the tumor tissues were irradiated with an 808 nm laser at a power density of 1.5 W/cm^2 for 3 min. (B) The appearances of the tumor sites of rGO or ArGO-treated

mice were monitored. (C) The tumor volumes were periodically measured using calipers until day 19. *Significantly different ($p < 0.05$) from the other groups (assessed by the ANOVA and the Student–Newman–Keuls test).

Fig. 8. Photothermal antitumor effect of the ArGO nanosheets.

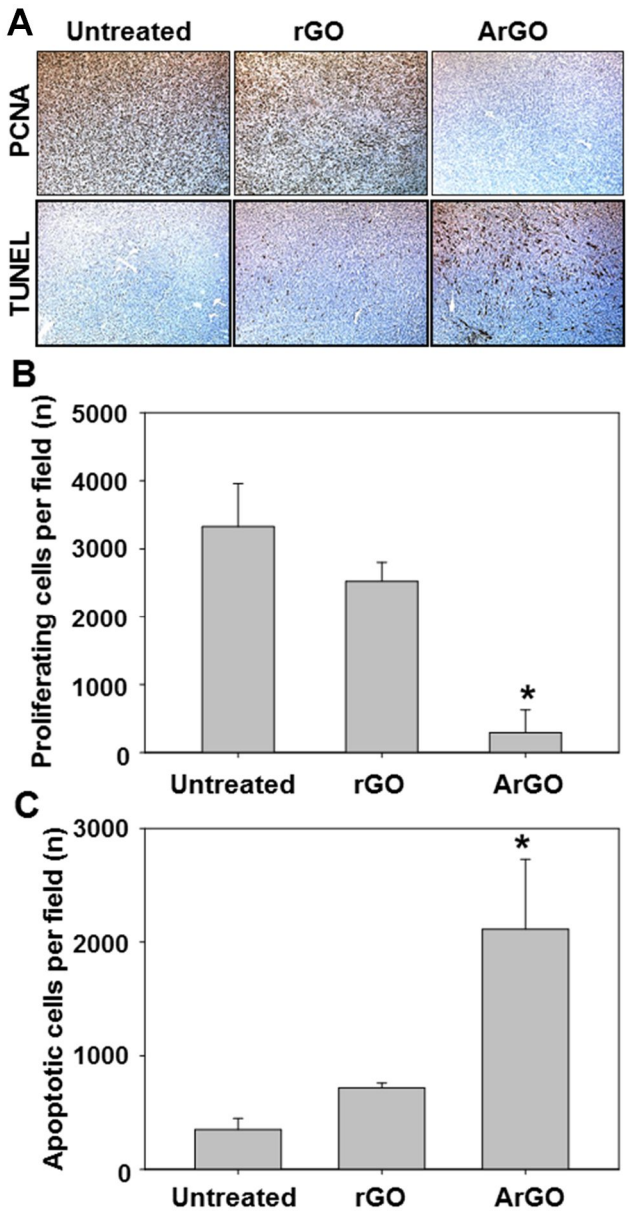

(A) Immunohistochemistry of tumor tissues. Tumor tissues were excised and sectioned for anti-PCNA antibody immunostaining and TUNEL assay.

The numbers of PCNA-immunostained proliferating cells (B) and TUNEL-labeled apoptotic cells (C) in isolated tumor tissues were determined by using Image-Pro® Plus software. *Significantly different ($p < 0.05$) from the other groups (assessed by the ANOVA and the Student–Newman–Keuls test).

IV. Discussion

This study demonstrated that surface modification of rGO nanosheets with APGA provides much higher biocompatibility and delivery rate for in vivo application of nano-graphenes. The rGO nanosheets coated with APGA revealed improved dispersion stability and consequent higher in vivo safety, pharmacokinetic property, and tumor accumulation as compared than plain rGO nanosheets.

Physical mixture of γ-PGA and rGO did absolutely not mitigate dispersion instability of rGO under physiological conditions, whereas non-covalent modification of APGA on rGO nanosheets contributed to greater dispersion stability in physiological conditions (Fig. 3). These results demonstrated rational design of tethering moiety should be considered for effective modification of graphene surface. For surface modification of rGO nanosheets with γ-PGA, phenyalanine residue was conjugated and utilized as a non-covalent anchoring moiety to nano-graphene surface. The aromatic ring of phenylalanine has been reported to bind on planar surface of graphenes via π–π interaction [Rajesh et al., 2009; Kim et al., 2011]. Our previous studies have demonstrated that various molecules containing aromatic structures such

as phenylalanine [Shim et al., 2015], cholesterol [Miao et al., 2013b], taurocholic acid [Shim et al., 2014], single-stranded DNA [Kim et al., 2015]. Non-covalent anchoring has a merit in that the simple engineering of coating materials on nano-graphenes which can avoid the multi-step covalent modification process including chemical conjugation of nano-graphenes [Shim et al., 2015].

Coating of APGA significantly lengthened stable period of rGO dispersion under physiological conditions over 4 weeks (Fig.3A). APGA would protect surface of rGO nanosheets against unsought biological interactions owing to its unique properties. In contrast with universal poly amino acids, γ-PGA has peculiar peptide linkages which are resistant to common proteases (Ogunleye et al., 2015). Moreover, polysaccharides-like homopolymeric structure of γ-PGA can avoid immune system as a protective extracellular matrix of bacteria (Kubler-Kielb et al., 2006). Our results also demonstrates propriety of APGA as a surface stabilizer, showing that APGA did not alter general features of graphene such as photothermal ability (Fig. 2) and cellular uptake efficiency (data now shown).

Biocompatible rGO revealed improved pharmacokinetic profiles (Fig.

4) and tumor accumulation (Fig. 5) due to protection effect of APGA during circulation. ArGO can eliminate the possibility of interaction between graphene nanosheets and blood components such as ions, serum proteins (Fig.3A), and RBC (Fig.3B), which lead to rapid clearance after systemic administration. Although tail vein injection of rGO alone revealed tumor accumulation due to enhanced permeable retention effect, APGA coating facilitated long circulation of rGO and consequently improved tumor accumulation after 24h (Fig. 4B).

ArGO itself revealed greater antitumor effect in SCC7 tumor-bearing mice via photothermal ability of rGO (Fig. 7). The rGO nanosheets are superior in photothermal ability to GO nanosheets due to improved photo-absorbance of its restored planar structures (Robinson et al., 2011; Turcheniuk et al., 2015). Moreover, rGO nanosheets are quite capable of loading hydrophobic (Shim et al., 2015) or aromatic (Miao et al., 2013b) cargos owing to maximized π–π stacking capacity as compared than GO nanosheets. Therefore, ArGO might be utilized as a nano-platform for combined anticancer treatment such as photothermal-chemotherapy, facilitating reduction of dosage and synergistic antitumor efficacy.

V. Conclusion

Non-covalent interaction of APGA with rGO did not alter structural and photothermal properties of graphene but remarkably improved biocompatibility of rGO under in vivo situations. ArGO exhibit greater in vivo safety and increased therapeutic index of plain rGO, indicating that the biocompatible graphene would be useful delivery nanoplatform for graphene-based nanomedicine.

논 문 초 록

현재 나노 전달체인 그래핀 (graphene)을 이용하여 다양한 질병 치료 방법들이 개발 되었지만 아직 남아있는 어려움은 그래핀의 생체적합성이 낮다는 점이다.

이 논문에서는 폴리-감마-글루탐산을 이용하여 그래핀에 코팅 시켜주면 혈중안정도와 생체적합성이 높아지는 것을 확인 할 수 있다. 글루탐산은 박테리아의 표면에서 찾아볼 수 있는 물질로 생체에 거부반응을 일으키지 않기 때문에 그래핀의 생체적합성을 높여주는 물질로 사용하였다.

길어진 폴리-감마-글루탐산이 코팅된 그래핀의 혈중 순환 시간이 길어지면서 원하는 부위인 암 주위에 더 많이 도달하게 됨으로 더 효과적인 광열항암치료를 할 수 있게 되었고 폴리-감마-글루탐산으로 그래핀을 코팅하여도 그래핀이 가지고 있는 특성을 저해시키지 않는다는 점 또한 추가적인 장점으로 볼 수 있다.

그 결과 폴리-감마-글루탐산으로 코팅한 그래핀이 코팅하지 않은 그래핀보다 8.6 배의 세포증식 결과 수치를 보였고 세포자살수치 또한 폴리-감마-글루탐산으로 코팅한 그래핀이

그렇지 않은 그래핀에 비교하였을 때 2.9 배의 세포자살 수치를 보였다.

이처럼 본 연구에서는 폴리-감마-글루탐산으로 그래핀을 코팅하여 광열치료를 함으로써 더 효과적인 항암치료 기대할 수 있는 가능성을 보여준다.

Keywords: Poly gamma glutamic acid derivative, Graphene nanosheets, Reduced graphene oxide, Surface functionalization, In vivo safety, Photothermal therapy, Anticancer therapy

학번 : 2014-24865

VI. References

1. Bajaj, Ishwar, and Rekha Singhal. "Poly (glutamic acid)–an emerging biopolymer of commercial interest." *Bioresource Technology* 102.10 (2011): 5551-5561.

2. Shen, Ai-Jun, et al. "Multifunctional nanocomposite based on graphene oxide for in vitro hepatocarcinoma diagnosis and treatment." *Journal of Biomedical Materials Research Part A* 100.9 (2012): 2499-2506.

3. Miao, Wenjun, et al. "Structure-dependent photothermal anticancer effects of carbon-based photoresponsive nanomaterials." *Biomaterials* 35.13 (2014): 4058-4065.

4. Wang, Zonghua, et al. "Fabrication and characterization of a triple functionalization of graphene oxide with Fe 3 O 4, folic acid and doxorubicin as dual-targeted drug nanocarrier." *Colloids and Surfaces B: Biointerfaces* 106 (2013): 60-65.

5. Sasidharan, Abhilash, et al. "Hemocompatibility and macrophage response of pristine and functionalized graphene." *Small* 8.8 (2012): 1251-1263.

6. Duch, Matthew C., et al. "Minimizing oxidation and stable nanoscale dispersion improves the biocompatibility of graphene in the lung." *Nano letters* 11.12 (2011): 5201-5207.

7. Duch, Matthew C., et al. "Minimizing oxidation and stable nanoscale dispersion improves the biocompatibility of graphene in the lung." *Nano letters* 11.12 (2011): 5201-5207.

8. Xu, Shun, Zheyu Zhang, and Maoquan Chu. "Long-term toxicity of reduced graphene oxide nanosheets: effects on female mouse reproductive ability and offspring development." *Biomaterials* 54 (2015): 188-200.

9. Jachak, Ashish C., et al. "Biological interactions and safety of graphene materials." *Mrs Bulletin* 37.12 (2012): 1307-1313.

10. Shim, Gayong, et al. "Reduced graphene oxide nanosheets coated with an anti-angiogenic anticancer low-molecular-weight heparin derivative for delivery of anticancer drugs." *Journal of Controlled Release* 189 (2014): 80-89.

11. Miao, Wenjun, et al. "Safety and tumor tissue accumulation of pegylated graphene oxide nanosheets for co-delivery of anticancer drug and photosensitizer." *Biomaterials* 34.13 (2013): 3402-3410.

12. Li, Yingjie, et al. "Surface Coating-Dependent Cytotoxicity and Degradation of Graphene Derivatives: Towards the Design of Non-Toxic, Degradable Nano-Graphene." *Small* 10.8 (2014): 1544-1554.

13. Sheng, Zonghai, et al. "Protein-assisted fabrication of nano-reduced graphene oxide for combined in vivo photoacoustic imaging and photothermal therapy."*Biomaterials* 34.21 (2013): 5236-5243.

14. Rajesh, Chinagandham, et al. "A theoretical study on the interaction of aromatic amino acids with graphene and single walled carbon nanotube." *The Journal of chemical physics* 130.12 (2009): 124911.

15. Kim, Sang N., et al. "Preferential binding of peptides to graphene edges and planes." *Journal of the American Chemical Society* 133.37 (2011): 14480-14483.

16. Ogunleye, Adetoro, et al. "Poly-γ-glutamic acid: production, properties and applications." *Microbiology* 161.1 (2015): 1-17.

17. Bajaj, Ishwar, and Rekha Singhal. "Poly (glutamic acid)–an emerging biopolymer of commercial interest." *Bioresource Technology* 102.10 (2011): 5551-5561.

18. Kocianova, Stanislava, et al. "Key role of poly-γ-DL-glutamic acid in immune evasion and virulence of Staphylococcus epidermidis." *The Journal of clinical investigation* 115.3 (2005): 688-694.

19. Foster, Timothy J. "Immune evasion by staphylococci." *Nature Reviews Microbiology* 3.12 (2005): 948-958.

20. Scorpio, Angelo, et al. "Poly-γ-glutamate capsule-degrading enzyme treatment enhances phagocytosis and killing of encapsulated Bacillus anthracis."*Antimicrobial agents and chemotherapy* 51.1 (2007): 215-222.

21. Jang, Jeyoun, et al. "The poly-γ-D-glutamic acid capsule of Bacillus anthracis enhances lethal toxin activity." *Infection and immunity* 79.9 (2011): 3846-3854.

22. Miao, Wenjun, et al. "Cholesteryl hyaluronic acid-coated, reduced graphene oxide nanosheets for anti-cancer drug delivery." *Biomaterials* 34.37 (2013): 9638-9647.

23. Wang, Li, et al. "Hierarchical nanocomposites of polyaniline nanowire arrays on reduced graphene oxide sheets for supercapacitors." *Scientific reports* 3 (2013).

24. Yuan, Honglun, et al. "Poly-γ-glutamic acid modified magnetic nanoparticles for fast solid phase extraction of trace amounts of Cu (ii) and Pb (ii)." *Analytical Methods* 6.24 (2014): 9800-9806.

25. Shim, Gayong, et al. "Functionalization of nano-graphenes by chimeric peptide engineering." *RSC Advances* 5.62 (2015): 49905-49913.

26. Kim, Mi-Gyeong, et al. "Polyaptamer DNA nanothread-anchored, reduced graphene oxide nanosheets for targeted delivery." *Biomaterials* 48 (2015): 129-136.

27. Kubler-Kielb, Joanna, et al. "Additional conjugation methods and immunogenicity of Bacillus anthracis poly-γ-D-glutamic acid-protein conjugates." *Infection and immunity* 74.8 (2006): 4744-4749.

28. Robinson, Joshua T., et al. "Ultrasmall reduced graphene oxide with high near-infrared absorbance for photothermal therapy." *Journal of the American Chemical Society* 133.17 (2011): 6825-6831.

29. Turcheniuk, Kostiantyn, et al. "Infrared Photothermal Therapy with Water Soluble Reduced Graphene Oxide: Shape, Size and Reduction Degree Effects." *Nano LIFE* 5.01 (2015): 1540002.

30. Stevanovic, Magdalena, et al. "Effect of poly-alpha, gamma, L-glutamic acid as a capping agent on morphology and oxidative stress-dependent toxicity of silver nanoparticles." *Int J Nanomed* 6 (2011): 2837-2847.